Longitudinal spin Seebeck effect in various garnet ferrites

K. Uchida,[1,2,*] T. Nonaka,[1] T. Kikkawa,[1] Y. Kajiwara,[1] and E. Saitoh[1,3,4,5]
[1]*Institute for Materials Research, Tohoku University, Sendai 980-8577, Japan*
[2]*PRESTO, Japan Science and Technology Agency, Saitama 332-0012, Japan*
[3]*WPI Advanced Institute for Materials Research, Tohoku University, Sendai 980-8577, Japan*
[4]*CREST, Japan Science and Technology Agency, Tokyo 102-0076, Japan*
[5]*Advanced Science Research Center, Japan Atomic Energy Agency, Tokai 319-1195, Japan*
(Received 6 February 2013; published 22 March 2013)

The longitudinal spin Seebeck effect (LSSE) is investigated in various garnet ferrites $Y_{3-x}R_xFe_{5-y}M_yO_{12}$ (R = Gd, Ca; M = Al, Mn, V, In, Zr) by means of the inverse spin Hall effect in Pt films. The magnitude of the LSSE voltage in the Pt/$Y_{3-x}R_xFe_{5-y}M_yO_{12}$ samples is found to be enhanced with increasing concentration of Fe in the garnet ferrites, which can be explained by a change in the spin-mixing conductance at the Pt/$Y_{3-x}R_xFe_{5-y}M_yO_{12}$ interfaces. We also investigate the dependence of the LSSE voltage on macroscopic magnetic parameters of $Y_{3-x}R_xFe_{5-y}M_yO_{12}$. The experimental results show that the LSSE voltage in the Pt/$Y_{3-x}R_xFe_{5-y}M_yO_{12}$ samples has a positive correlation with the Curie temperature and the saturation magnetization, but no clear correlation with the gyromagnetic ratio and the Gilbert damping constant of the samples.

DOI: 10.1103/PhysRevB.87.104412 PACS number(s): 85.75.−d, 72.25.−b, 72.15.Jf

I. INTRODUCTION

Spin caloritronics is a branch of spintronics that focuses on the interaction among spin, charge, and heat currents.[1–3] A main purpose of spin caloritronics is to develop novel thermo-spin effects and strategies to improve thermoelectric devices. Important discoveries in this field include spin-dependent Seebeck/Peltier effects in magnetic nanostructures,[4,5] thermal spin injection into silicon,[6] magnonic thermal Hall effects,[7] thermal spin transfer torques,[8] and spin Seebeck effects (SSEs).[9–32]

The SSE refers to the generation of a spin voltage as a result of a temperature gradient in magnetic materials. Here, spin voltage is a potential for electrons' spins to drive a nonequilibrium spin current; when a conductor is attached to a magnet with a finite spin voltage, it induces a spin injection into the conductor. The SSE has attracted much attention in spintronics and spin caloritronics, since it enables simple and versatile generation of a spin current from heat.

Recent experiments show that the SSE is a versatile phenomenon in magnetic materials; it was observed not only in electrical conductors[9–11,14,20,21,31] but also in insulators.[13,15–17,24,28,31,32] However, most SSE experiments to date have been performed only in a few materials, such as $Ni_{81}Fe_{19}$, GaMnAs, and $Y_3Fe_5O_{12}$ (YIG).[23] In this paper, we report the observation of the SSE in more than 20 garnet ferrites with various compositions and investigate the dependence of the SSE signals on the concentration of constituent elements and on macroscopic magnetic parameters of the garnet ferrites. These systematic measurements will provide guidance for complete understanding of the physics of the SSE and for discovering materials with large thermo-spin conversion efficiency.

II. EXPERIMENTAL PROCEDURE

For the systematic investigation of the SSE in various garnet ferrites, we employed a longitudinal configuration,[15,17,23,30] which is the simplest and most straightforward structure for measuring the SSE in insulators. Figure 1(a) shows a schematic illustration of the longitudinal SSE (LSSE) device; it comprises a ferrimagnetic insulator (FI) slab covered with a paramagnetic metal (PM) film. When a temperature gradient ∇T is applied over the FI layer perpendicular to the PM/FI interface (z direction), a spin voltage is thermally generated and injects a spin current with the spatial direction $\mathbf{J}_s$ and the spin-polarization vector $\boldsymbol{\sigma}$ into the PM layer, where $\mathbf{J}_s$ and $\boldsymbol{\sigma}$ are along the ∇T direction and the magnetization $\mathbf{M}$ of FI, respectively [Fig. 1(b)]. This spin current is converted into an electric field $\mathbf{E}_{ISHE}$ by the inverse spin Hall effect (ISHE) in the PM layer.[33–42] When $\mathbf{M}$ is along the x direction, $\mathbf{E}_{ISHE}$ is generated along the y direction according to the relation

$$\mathbf{E}_{ISHE} \propto \mathbf{J}_s \times \boldsymbol{\sigma}. \quad (1)$$

Therefore, by measuring $\mathbf{E}_{ISHE}$ in the PM layer, one can detect the LSSE electrically [Fig. 1(b)].

The sample used in the present study consists of a ferrimagnetic garnet ferrite $Y_{3-x}R_xFe_{5-y}M_yO_{12}$ (R = Gd, Ca; M = Al, Mn, V, In, Zr) slab (FI layer), of which the host material is YIG, and a Pt film (PM layer). The $Y_{3-x}R_xFe_{5-y}M_yO_{12}$ slabs are polycrystalline, prepared by a press sintering method (made by Mitsubishi Electric Metecs Co., Ltd.). Table I shows the atomic percentage of constituent elements in $Y_{3-x}R_xFe_{5-y}M_yO_{12}$, measured by inductively coupled plasma-atomic emission spectroscopy. All the $Y_{3-x}R_xFe_{5-y}M_yO_{12}$ slabs provide excellent electrical insulation. The top surface of the $Y_{3-x}R_xFe_{5-y}M_yO_{12}$ slabs was well polished by mechanical and chemical-mechanical polishing methods. The Pt films were then sputtered on the polished surface of the $Y_{3-x}R_xFe_{5-y}M_yO_{12}$ slabs all at the same time. The lengths of the $Y_{3-x}R_xFe_{5-y}M_yO_{12}$ slabs (Pt films) along the x, y, and z directions are 6 mm (6 mm), 2 mm (2 mm), and 1 mm (10 nm), respectively. A temperature gradient ∇T was applied parallel to the z direction by sandwiching the sample between two Cu plates (see Fig. 3 of Ref. 23), where the temperature of the upper (lower) Cu plate was stabilized at 320 K (300 K). Here, to reduce thermal

 ©2013 American Physical Society

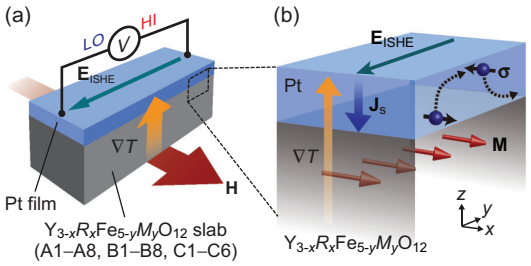

FIG. 1. (Color online) (a) A schematic illustration of the Pt/$Y_{3-x}R_xFe_{5-y}M_yO_{12}$ sample. (b) Measurement mechanism of the LSSE by means of the ISHE. ∇T, **H**, **M**, $\mathbf{E}_{\mathrm{ISHE}}$, $\mathbf{J}_s$, and $\boldsymbol{\sigma}$ denote the temperature gradient, external magnetic-field vector (with the magnitude H), magnetization vector of the $Y_{3-x}R_xFe_{5-y}M_yO_{12}$ slab, electric field induced by the ISHE, spatial direction of the thermally generated spin current, and spin-polarization vector of electrons in the Pt film, respectively.

contact resistance between the sample and the Cu plates, thermal grease was applied between them. To measure the LSSE in the Pt/$Y_{3-x}R_xFe_{5-y}M_yO_{12}$ samples, we measure an electric voltage difference V between the ends of the Pt layer of the samples with applying an external magnetic field H along the x direction, as illustrated in Fig. 1(a).

Hereafter, the samples are divided into three groups (Groups A–C) in terms of constituent elements in $Y_{3-x}R_xFe_{5-y}M_yO_{12}$; as shown in Table I, A1–A8 in Group A refer to the samples including Al and Mn (M = Al, Mn), B1–B8 in Group B to the samples including Gd, Al, and Mn (R = Gd; M = Al, Mn), and C1–C6 in Group C to the samples including Ca, Mn, V, In, and Zr (R = Ca; M = Mn, V, In, Zr).

III. RESULTS AND DISCUSSION

Figure 2 shows the electric voltage V in the Pt/$Y_{3-x}R_xFe_{5-y}M_yO_{12}$ samples at the temperature difference $\Delta T = 20$ K as a function of the magnetic field H. In all the samples, we observed clear V signals of which the sign is reversed by reversing H. This result indicates that the V signals are affected by the magnetization direction of the $Y_{3-x}R_xFe_{5-y}M_yO_{12}$ slab, i.e., the spin-polarization vector in the Pt layer, a situation consistent with Eq. (1) [Fig. 1(b)]. Since the $Y_{3-x}R_xFe_{5-y}M_yO_{12}$ samples used in the present study are very good insulators, conventional thermoelectric artifacts in $Y_{3-x}R_xFe_{5-y}M_yO_{12}$ do not exist at all. Furthermore, the extrinsic signals induced by a static magnetic proximity effect[43] at the Pt/$Y_{3-x}R_xFe_{5-y}M_yO_{12}$ interface is negligibly small[28,31,44] (note that the saturation magnetization of $Y_{3-x}R_xFe_{5-y}M_yO_{12}$ is comparable to or smaller than that of pure YIG, as shown in Table I). Therefore, we can conclude that the voltage signals observed in the Pt/$Y_{3-x}R_xFe_{5-y}M_yO_{12}$ samples are due to the ISHE induced by the LSSE.

In Fig. 3, we plot the magnitude of the LSSE voltage per unit temperature difference $|V_{\mathrm{LSSE}}/\Delta T|$ in the Pt/$Y_{3-x}R_xFe_{5-y}M_yO_{12}$ samples as a function of the

TABLE I. Atomic percentages of constituent elements and magnetic parameters of $Y_{3-x}R_xFe_{5-y}M_yO_{12}$. The horizontal lines (—) mean that the concentration of elements is less than 0.005 at. %. T_c, $4\pi M_s$, γ, and α denote the Curie temperature, the saturation magnetization, the gyromagnetic ratio, and the Gilbert damping constant of $Y_{3-x}R_xFe_{5-y}M_yO_{12}$, respectively. γ and α are estimated from the ferromagnetic resonance (FMR) experiments (see Appendix for details).

Garnet ferrite		Atomic percentage (at. %)									Magnetic parameter			
		Y	Gd	Ca	Fe	Al	Mn	V	In	Zr	T_c (K)	$4\pi M_s$ (G)	γ ($G^{-1}s^{-1}$)	α
Group A	A1	15.10	—	—	19.37	5.29	0.23	—	—	—	407	444	1.81×10^7	1.32×10^{-3}
	A2	15.24	—	—	19.76	4.88	0.11	—	—	—	429	542	1.85×10^7	1.58×10^{-3}
	A3	15.21	—	—	20.67	4.11	0.01	—	—	—	458	672	1.82×10^7	3.07×10^{-3}
	A4	15.16	—	—	21.17	3.41	0.26	—	—	—	455	825	1.82×10^7	1.04×10^{-3}
	A5	15.26	—	—	21.54	2.65	0.55	—	—	—	487	1025	1.84×10^7	1.39×10^{-3}
	A6	15.20	—	—	22.86	1.93	0.01	—	—	—	511	1214	1.84×10^7	0.95×10^{-3}
	A7	15.18	—	—	23.73	0.61	0.49	—	—	—	539	1578	1.83×10^7	7.52×10^{-3}
	A8	15.19	—	—	24.72	0.01	0.08	—	—	—	554	1813	1.72×10^7	1.43×10^{-3}
Group B	B1	11.54	3.26	—	21.86	3.25	0.08	—	—	—	481	632	1.84×10^7	3.14×10^{-3}
	B2	11.38	3.51	—	23.91	1.18	0.03	—	—	—	566	988	1.87×10^7	2.03×10^{-3}
	B3	9.43	5.50	—	23.96	1.00	0.11	—	—	—	529	824	1.85×10^7	7.69×10^{-3}
	B4	13.02	1.99	—	24.49	0.39	0.11	—	—	—	547	1436	1.83×10^7	4.57×10^{-3}
	B5	10.51	4.30	—	24.54	0.07	0.58	—	—	—	552	1278	1.90×10^7	3.84×10^{-3}
	B6	13.45	1.50	—	24.91	0.11	0.03	—	—	—	559	1589	1.78×10^7	5.13×10^{-3}
	B7	8.25	6.65	—	24.91	0.08	0.11	—	—	—	535	1014	1.81×10^7	3.48×10^{-3}
	B8	10.47	4.44	—	24.97	0.09	0.03	—	—	—	555	1267	1.90×10^7	3.10×10^{-3}
Group C	C1	7.91	—	6.98	19.82	—	0.06	3.67	1.56	0.01	464	806	1.82×10^7	0.95×10^{-3}
	C2	8.89	—	5.99	19.96	—	0.07	3.14	1.95	0.01	453	1011	1.84×10^7	1.84×10^{-3}
	C3	9.44	—	5.51	21.98	—	0.21	2.84	0.01	—	558	810	1.79×10^7	4.40×10^{-3}
	C4	13.04	—	2.02	22.46	—	0.09	1.00	1.40	—	498	1614	1.88×10^7	3.79×10^{-3}
	C5	10.54	—	4.45	22.47	—	0.21	2.31	0.02	—	551	1005	1.80×10^7	0.97×10^{-3}
	C6	13.27	—	1.79	23.03	—	0.08	0.01	0.02	1.82	485	1983	1.84×10^7	2.41×10^{-3}

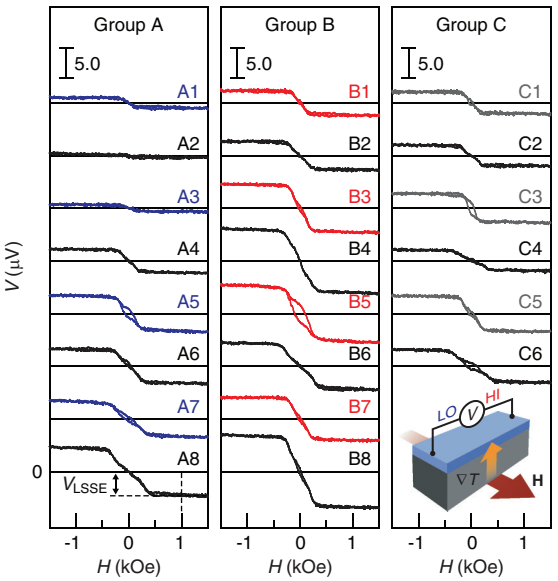

FIG. 2. (Color online) H dependence of the voltage V in the Pt/$Y_{3-x}R_xFe_{5-y}M_yO_{12}$ samples at the temperature difference ΔT = 20 K. The labels A1–C6 refer to the species of the garnet ferrites (see Table I).

concentration (atomic percentage) of constituent elements in $Y_{3-x}R_xFe_{5-y}M_yO_{12}$, where V_{LSSE} is defined as V at $H = 1$ kOe. We found that the LSSE voltage exhibits a tendency to increase with increasing concentration of Fe atoms in $Y_{3-x}R_xFe_{5-y}M_yO_{12}$ [Fig. 3(a)]. This positive correlation was observed to appear in all the sample groups (Groups A–C), indicating that the species of substituted elements in $Y_{3-x}R_xFe_{5-y}M_yO_{12}$ is not essential. In fact, although the SSE voltage has no correlation with the concentration of each substituted elements at the Y and Fe sites in $Y_{3-x}R_xFe_{5-y}M_yO_{12}$ [Figs. 3(c) and 3(d)], a clear negative correlation was observed between the LSSE voltage and the total concentration of the substituted elements at the Fe site [Fig. 3(b)]. Note that, in Groups A and B, the LSSE has a negative correlation with the concentration of Al since Fe atoms are substituted mainly by Al atoms [see Fig. 3(d) and Table I].

We now provide a qualitative discussion on the positive correlation between the LSSE voltage and the concentration of Fe atoms in the Pt/$Y_{3-x}R_xFe_{5-y}M_yO_{12}$ samples. Previous studies on the SSE revealed that the conversion efficiency from a temperature gradient into the SSE voltage is determined by the following three factors: (1) the spin Hall angle in PM, (2) the difference between an effective magnon temperature in FI and an effective electron temperature in PM, and (3) the spin-mixing conductance at the PM/FI interface. Factor (1) is irrelevant to the positive correlation observed here since the PM layer of all the samples is Pt. We believe that factor (2) is also irrelevant to this positive correlation. This is because

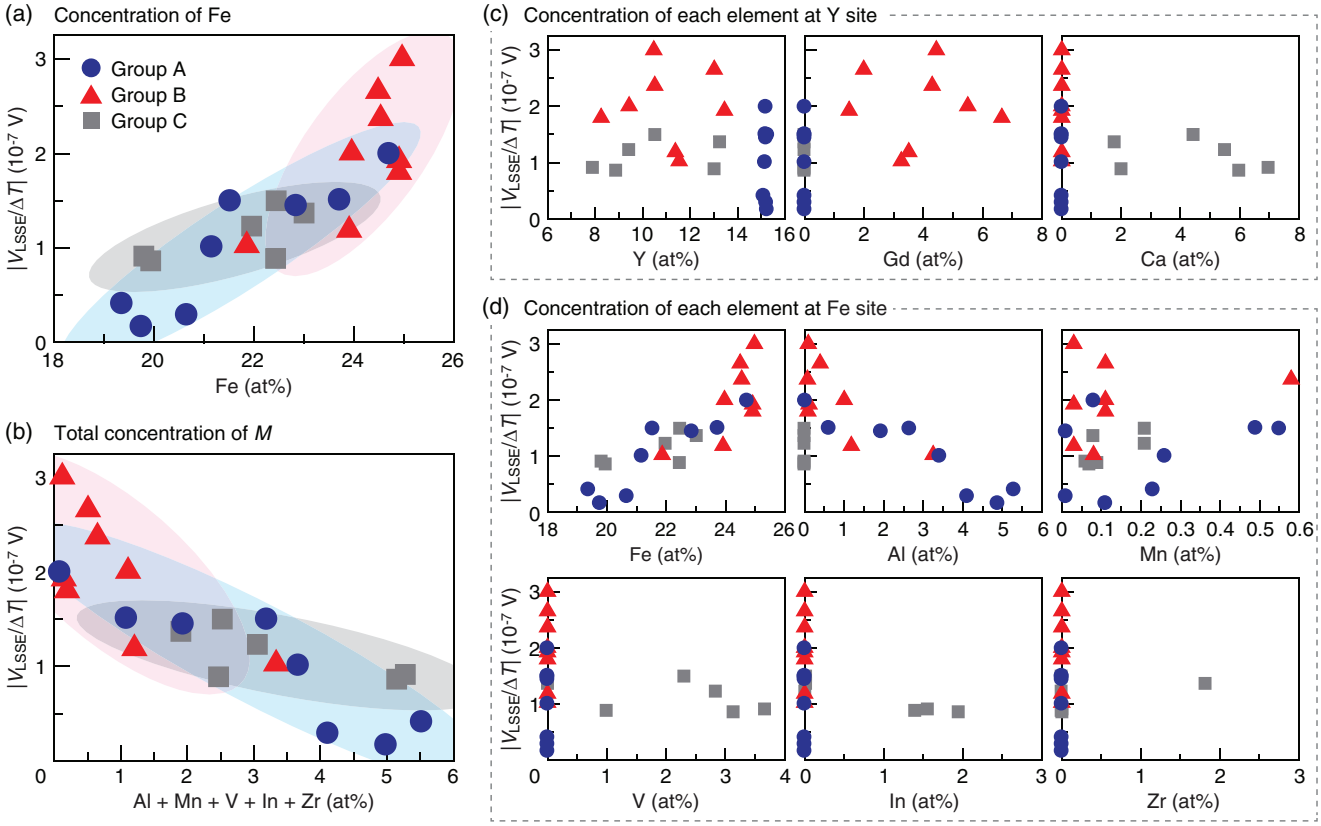

FIG. 3. (Color online) The LSSE voltage per unit temperature difference $|V_{LSSE}/\Delta T|$ in the Pt/$Y_{3-x}R_xFe_{5-y}M_yO_{12}$ samples as a function of the atomic percentage of (a) Fe, (b) the total of the substituted elements at the Fe site (Al, Mn, V, In, Zr), (c) each element at the Y site (Y, Gd, Ca), and (d) each element at the Fe site (Fe, Al, Mn, V, In, Zr) in $Y_{3-x}R_xFe_{5-y}M_yO_{12}$. V_{LSSE} is defined as V at $H = 1$ kOe (see Fig. 2). The colored ellipses in (a) and (b) represent 68% confidence regions, where the blue, red, and gray ellipses correspond to the data for Groups A, B, and C, respectively.

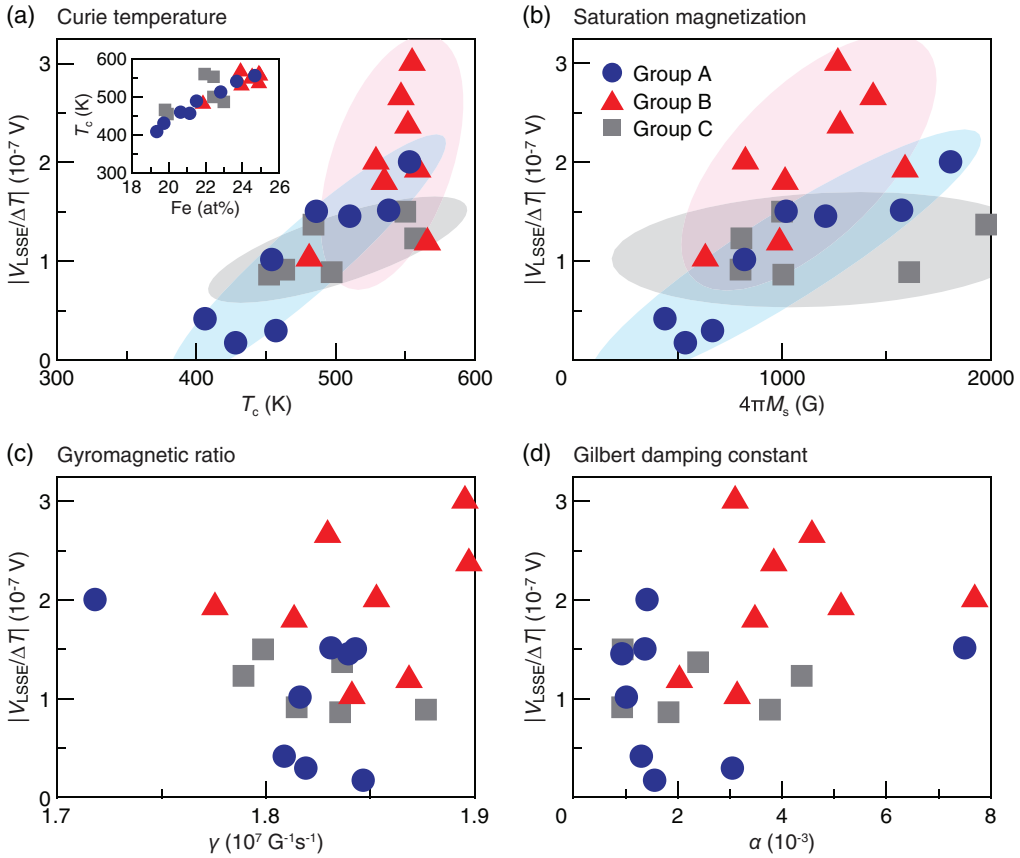

FIG. 4. (Color online) $|V_{LSSE}/\Delta T|$ in the Pt/$Y_{3-x}R_xFe_{5-y}M_yO_{12}$ samples as a function of (a) the Curie temperature T_c, (b) the saturation magnetization $4\pi M_s$, (c) the gyromagnetic ratio γ, and (d) the Gilbert damping constant α of $Y_{3-x}R_xFe_{5-y}M_yO_{12}$. The inset to (a) shows the dependence of T_c on the Fe concentration in $Y_{3-x}R_xFe_{5-y}M_yO_{12}$.

the effective magnon-electron temperature difference in the longitudinal configuration was shown to be induced by the electron-phonon interaction in PM and nonequilibrium phonon transport through FI,[15,23,29,30] which are indirectly related to the concentration of Fe atoms in FI. In contrast, factor (3) is directly associated with the Fe concentration in FI; a recently reported theory based on first-principles calculation shows that the spin-mixing conductance monotonically increases with increasing magnetic moment density at the PM/FI interface,[45] which can explain the experimental behavior of the LSSE voltage in the present Pt/$Y_{3-x}R_xFe_{5-y}M_yO_{12}$ samples shown in Fig. 3(a).

Next, we investigate the dependence of the LSSE voltage on macroscopic magnetic parameters of $Y_{3-x}R_xFe_{5-y}M_yO_{12}$. Table I also shows the Curie temperature T_c, the saturation magnetization $4\pi M_s$, the gyromagnetic ratio γ, and the Gilbert damping constant α of $Y_{3-x}R_xFe_{5-y}M_yO_{12}$, where T_c was measured with a vibrating sample magnetometer, $4\pi M_s$ was with an M-H curve tracer, and γ and α were estimated from ferromagnetic resonance (FMR) measurements (see Appendix). We found that $|V_{LSSE}/\Delta T|$ also tends to increase with increasing T_c and $4\pi M_s$ of $Y_{3-x}R_xFe_{5-y}M_yO_{12}$, since there is a positive correlation among the Fe concentration, T_c, and $4\pi M_s$ in these samples [Figs. 4(a) and 4(b)]. In contrast, no clear correlation was observed among $|V_{LSSE}/\Delta T|$, γ, and α [Figs. 4(c) and 4(d)], indicating that the LSSE voltage is irrelevant to spin-orbit interaction (related to γ) and magnon lifetime (related to α) in $Y_{3-x}R_xFe_{5-y}M_yO_{12}$. This result is not contrary to the aforementioned interpretation that the thermally generated spin voltage in the longitudinal configuration is attributed to the electron-phonon interaction and phonon propagations.[15,23,29,30]

IV. SUMMARY

In the present study, we measured the longitudinal spin Seebeck effect (LSSE) in polycrystalline $Y_{3-x}R_xFe_{5-y}M_yO_{12}$ (R = Gd, Ca; M = Al, Mn, V, In, Zr) slabs by means of the inverse spin Hall effect in Pt films. The magnitude of the LSSE voltage in the Pt/$Y_{3-x}R_xFe_{5-y}M_yO_{12}$ samples was observed to increase with increasing Fe concentration in $Y_{3-x}R_xFe_{5-y}M_yO_{12}$. This correlation between the LSSE voltage and the Fe concentration can be attributed to a change in the spin-mixing conductance at the Pt/$Y_{3-x}R_xFe_{5-y}M_yO_{12}$ interfaces. The observed dependence of the LSSE voltage on macroscopic magnetic parameters reveals that the LSSE in the Pt/$Y_{3-x}R_xFe_{5-y}M_yO_{12}$ samples has a positive correlation with the Curie temperature and the saturation magnetization of $Y_{3-x}R_xFe_{5-y}M_yO_{12}$, while it has no clear correlation with the gyromagnetic ratio and the Gilbert damping constant estimated from FMR measurements. Since the experiments shown in this paper focus only on ferrimagnetic insulators with garnet structure, the measurements of the SSE in materials with

different crystal structures would be important in order to elucidate global behavior of the SSE.

ACKNOWLEDGMENTS

The authors thank S. Hirose and Y. Higuchi for valuable discussions on sample preparation. This work was supported by PRESTO-JST "Phase Interfaces for Highly Efficient Energy Utilization", CREST-JST "Creation of Nanosystems with Novel Functions through Process Integration", a Grant-in-Aid for Research Activity Start-up (No. 24860003) from MEXT, Japan, a Grant-in-Aid for Scientific Research (A) (No. 24244051) from MEXT, Japan, LC-IMR of Tohoku University, The Murata Science Foundation, The Mazda Foundation, and The Sumitomo Foundation.

APPENDIX: ESTIMATION OF GYROMAGNETIC RATIO AND GILBERT DAMPING CONSTANT

In this appendix, we show the details of the FMR measurements and analysis for estimating the gyromagnetic ratio γ and the Gilbert damping constant α of $Y_{3-x}R_xFe_{5-y}M_yO_{12}$. Before measuring FMR, the $Y_{3-x}R_xFe_{5-y}M_yO_{12}$ slabs were machined to a cylinder shape of 1 mm diameter and 1 mm height to simplify the estimation of demagnetizing factors in $Y_{3-x}R_xFe_{5-y}M_yO_{12}$.[46] A dc external magnetic field H was applied along the axis of the cylinder (z direction) and a microwave magnetic field was applied in the diametrical direction (x direction) by placing the sample on the center of a microstrip line connected to a vector network analyzer. The input microwave power was fixed at 20 mW. Under this condition, we measured the H dependence of the microwave transmission property $|S_{21}|^2$ on the changing microwave frequency f, where $|S_{21}|^2$ is defined as the ratio of the incident microwave power from port 1 of the vector network analyzer to the transmitted microwave power to port 2. By subtracting a dc offset and a linear background from the $|S_{21}|^2$ data, we obtained the spectra of the microwave absorption intensity I [see Fig. 5(a), the experimental data for the sample A8]. In the present configuration, only uniform FMR mode and magnetostatic forward volume waves (MSFVWs) are excited, where a sharp single peak (multiple peaks) in the higher (lower) H region in the I spectrum corresponds to the FMR (MSFVW) mode [Fig. 5(a)]. This simple spectrum shape allows us to analyze the FMR mode quantitatively. Here, by fitting the FMR spectrum with a Lorentzian function, we obtained the magnetic field at the FMR condition H_{FMR} and the FMR linewidth ΔH_{FWHM} (full width at half maximum, FWHM).

The gyromagnetic ratio was estimated by using the Kittel equation.[47] According to this equation, at the FMR condition, the microwave frequency satisfies

$$f = \frac{\gamma}{2\pi}\{[H_{FMR} + (N^x - N^z)M_s] \times [H_{FMR} + (N^y - N^z)M_s]\}^{\frac{1}{2}}, \quad \text{(A1)}$$

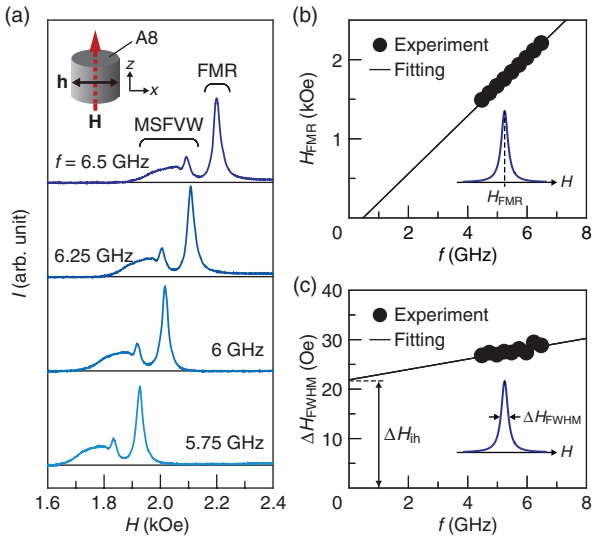

FIG. 5. (Color online) (a) H dependence of the microwave absorption intensity I for the sample A8. (b) and (c) The microwave frequency f dependence of (b) H_{FMR} and (c) ΔH_{FWHM}. Here, H_{FMR} and ΔH_{FWHM} denote the magnetic field at the FMR condition and the FMR linewidth, respectively. The solid lines in (b) and (c) are the fitting results based on Eqs. (A2) and (A3), respectively.

where N^x, N^y, and N^z are demagnetizing factors along the x, y, and z directions, respectively ($N^x + N^y + N^z = 4\pi$). Here, we take no account of crystal magnetic anisotropy of $Y_{3-x}R_xFe_{5-y}M_yO_{12}$ because the samples used here are polycrystalline. Since we can assume $N^z/4\pi = 0.27$ and $N^x/4\pi = N^y/4\pi = 0.365$ in the present cylinder shape,[46] Eq. (A1) becomes

$$H_{FMR} = \frac{2\pi}{\gamma} f - (0.095 \times 4\pi M_s). \quad \text{(A2)}$$

By fitting the experimental data on the f dependence of H_{FMR} with Eq. (A2), we obtained γ of $Y_{3-x}R_xFe_{5-y}M_yO_{12}$ [Fig. 5(b)], where the values of $4\pi M_s$ shown in Table I were used.

The Gilbert damping constant was quantified by using the FMR linewidth ΔH_{FWHM}.[42] In general, ΔH_{FWHM} is expressed as follows:[38]

$$\Delta H_{FWHM} = \frac{4\pi\alpha}{\gamma} f + \Delta H_{ih}, \quad \text{(A3)}$$

where ΔH_{ih} is the sample-dependent inhomogeneous linewidth, measured as the zero-frequency intercept. Based on Eq. (A3), we fitted the f dependence of ΔH_{FWHM} in $Y_{3-x}R_xFe_{5-y}M_yO_{12}$ with a linear function [Fig. 5(c)]. By using the values of γ obtained from Eq. (A2), we estimated α of $Y_{3-x}R_xFe_{5-y}M_yO_{12}$ from the slope of the linear function.

*kuchida@imr.tohoku.ac.jp

[1] M. Johnson and R. H. Silsbee, Phys. Rev. B **35**, 4959 (1987).

[2] *Spin Caloritronics*, edited by G. E. W. Bauer, A. H. MacDonald, and S. Maekawa, special issue of Solid State Commun. **150**, 459 (2010).

[3]G. E. W. Bauer, E. Saitoh, and B. J. van Wees, Nat. Mater. **11**, 391 (2012).
[4]A. Slachter, F. L. Bakker, J.-P. Adam, and B. J. van Wees, Nat. Phys. **6**, 879 (2010).
[5]J. Flipse, F. L. Bakker, A. Slachter, F. K. Dejene, and B. J. van Wees, Nat. Nanotech. **7**, 166 (2012).
[6]J.-C. Le Breton, S. Sharma, H. Saito, S. Yuasa, and R. Jansen, Nature (London) **475**, 82 (2011).
[7]Y. Onose, T. Ideue, H. Katsura, Y. Shiomi, N. Nagaosa, and Y. Tokura, Science **329**, 297 (2010).
[8]M. Hatami, G. E. W. Bauer, Q.-F. Zhang, and P. J. Kelly, Phys. Rev. Lett. **99**, 066603 (2007).
[9]K. Uchida, S. Takahashi, K. Harii, J. Ieda, W. Koshibae, K. Ando, S. Maekawa, and E. Saitoh, Nature (London) **455**, 778 (2008).
[10]K. Uchida, T. Ota, K. Harii, S. Takahashi, S. Maekawa, Y. Fujikawa, and E. Saitoh, Solid State Commun. **150**, 524 (2010).
[11]K. Uchida, T. Ota, K. Harii, K. Ando, H. Nakayama, and E. Saitoh, J. Appl. Phys. **107**, 09A951 (2010).
[12]J. Xiao, G. E. W. Bauer, K. Uchida, E. Saitoh, and S. Maekawa, Phys. Rev. B **81**, 214418 (2010).
[13]K. Uchida, J. Xiao, H. Adachi, J. Ohe, S. Takahashi, J. Ieda, T. Ota, Y. Kajiwara, H. Umezawa, H. Kawai, G. E. W. Bauer, S. Maekawa, and E. Saitoh, Nat. Mater. **9**, 894 (2010).
[14]C. M. Jaworski, J. Yang, S. Mack, D. D. Awschalom, J. P. Heremans, and R. C. Myers, Nat. Mater. **9**, 898 (2010).
[15]K. Uchida, H. Adachi, T. Ota, H. Nakayama, S. Maekawa, and E. Saitoh, Appl. Phys. Lett. **97**, 172505 (2010).
[16]H. Adachi, K. Uchida, E. Saitoh, J. Ohe, S. Takahashi, and S. Maekawa, Appl. Phys. Lett. **97**, 252506 (2010).
[17]K. Uchida, T. Nonaka, T. Ota, and E. Saitoh, Appl. Phys. Lett. **97**, 262504 (2010).
[18]H. Adachi, J. I. Ohe, S. Takahashi, and S. Maekawa, Phys. Rev. B **83**, 094410 (2011).
[19]J. I. Ohe, H. Adachi, S. Takahashi, and S. Maekawa, Phys. Rev. B **83**, 115118 (2011).
[20]C. M. Jaworski, J. Yang, S. Mack, D. D. Awschalom, R. C. Myers, and J. P. Heremans, Phys. Rev. Lett. **106**, 186601 (2011).
[21]S. Bosu, Y. Sakuraba, K. Uchida, K. Saito, T. Ota, E. Saitoh, and K. Takanashi, Phys. Rev. B **83**, 224401 (2011).
[22]K. Uchida, H. Adachi, T. An, T. Ota, M. Toda, B. Hillebrands, S. Maekawa, and E. Saitoh, Nat. Mater. **10**, 737 (2011).
[23]K. Uchida, T. Ota, H. Adachi, J. Xiao, T. Nonaka, Y. Kajiwara, G. E. W. Bauer, S. Maekawa, and E. Saitoh, J. Appl. Phys. **111**, 103903 (2012).
[24]A. Kirihara, K. Uchida, Y. Kajiwara, M. Ishida, Y. Nakamura, T. Manako, E. Saitoh, and S. Yorozu, Nat. Mater. **11**, 686 (2012).
[25]C. M. Jaworski, R. C. Myers, E. Johnston-Halperin, and J. P. Heremans, Nature (London) **487**, 210 (2012).
[26]Y. Ohnuma, H. Adachi, E. Saitoh, and S. Maekawa, Phys. Rev. B **87**, 014423 (2013).
[27]D. Qu, S. Y. Huang, J. Hu, R. Wu, and C. L. Chien, Phys. Rev. Lett. **110**, 067206 (2013).
[28]T. Kikkawa, K. Uchida, Y. Shiomi, Z. Qiu, D. Hou, D. Tian, H. Nakayama, X.-F. Jin, and E. Saitoh, Phys. Rev. Lett. **110**, 067207 (2013).
[29]H. Adachi, K. Uchida, E. Saitoh, and S. Maekawa, Rep. Prog. Phys. **76**, 036501 (2013).
[30]H. Adachi and S. Maekawa, J. Korean Phys. Soc. (to be published), arXiv:1209.0228.
[31]R. Ramos, T. Kikkawa, K. Uchida, H. Adachi, I. Lucas, M. H. Aguirre, P. Algarabel, L. Morellon, S. Maekawa, E. Saitoh, and M. R. Ibarra, Appl. Phys. Lett. **102**, 072413 (2013).
[32]D. Meier, T. Kuschel, L. Shen, A. Gupta, T. Kikkawa, K. Uchida, E. Saitoh, J.-M. Schmalhorst, and G. Reiss, Phys. Rev. B **87**, 054421 (2013).
[33]A. Azevedo, L. H. Vilela Leão, R. L. Rodriguez-Suarez, A. B. Oliveira, and S. M. Rezende, J. Appl. Phys. **97**, 10C715 (2005).
[34]E. Saitoh, M. Ueda, H. Miyajima, and G. Tatara, Appl. Phys. Lett. **88**, 182509 (2006).
[35]S. O. Valenzuela and M. Tinkham, Nature (London) **442**, 176 (2006).
[36]T. Kimura, Y. Otani, T. Sato, S. Takahashi, and S. Maekawa, Phys. Rev. Lett. **98**, 156601 (2007).
[37]K. Ando, Y. Kajiwara, S. Takahashi, S. Maekawa, K. Takemoto, M. Takatsu, and E. Saitoh, Phys. Rev. B **78**, 014413 (2008).
[38]O. Mosendz, V. Vlaminck, J. E. Pearson, F. Y. Fradin, G. E. W. Bauer, S. D. Bader, and A. Hoffmann, Phys. Rev. B **82**, 214403 (2010).
[39]K. Ando, S. Takahashi, J. Ieda, Y. Kajiwara, H. Nakayama, T. Yoshino, K. Harii, Y. Fujikawa, M. Matsuo, S. Maekawa, and E. Saitoh, J. Appl. Phys. **109**, 103913 (2011).
[40]H. Nakayama, K. Ando, K. Harii, T. Yoshino, R. Takahashi, Y. Kajiwara, K. Uchida, Y. Fujikawa, and E. Saitoh, Phys. Rev. B **85**, 144408 (2012).
[41]L. Liu, C.-F. Pai, Y. Li, H. W. Tseng, D. C. Ralph, and R. A. Buhrman, Science **336**, 555 (2012).
[42]R. Iguchi, K. Ando, R. Takahashi, T. An, E. Saitoh, and T. Sato, Jpn. J. Appl. Phys. **51**, 103004 (2012).
[43]S. Y. Huang, X. Fan, D. Qu, Y. P. Chen, W. G. Wang, J. Wu, T. Y. Chen, J. Q. Xiao, and C. L. Chien, Phys. Rev. Lett. **109**, 107204 (2012).
[44]H. Nakayama, M. Althammer, Y.-T. Chen, K. Uchida, Y. Kajiwara, D. Kikuchi, T. Ohtani, S. Geprägs, M. Opel, S. Takahashi, R. Gross, G. E. W. Bauer, S. T. B. Goennenwein, and E. Saitoh, arXiv:1211.0098.
[45]X. Jia, K. Liu, K. Xia, and G. E. W. Bauer, Europhys. Lett. **96**, 17005 (2011).
[46]R. M. Bozorth, *Ferromagnetism* (IEEE, Piscataway, NJ, 1993).
[47]C. Kittel, J. Phys. Radium **12**, 291 (1951).